Journal of Materials Chemistry C

ROYAL SOCIETY OF CHEMISTRY

PAPER

View Article Online
View Journal | View Issue

Cite this: *J. Mater. Chem. C*, 2026, **14**, 833

Pursuing red thermally activated delayed fluorescence upon increasing the degree of branching in phenothiazine-trithienyltriazine push–pull compounds

Pietro Mancini,†[a] Chiara Montanari,†[a] Kusum Yadav,†[b] Erica Luzi,[a] Rajneesh Misra *[b] and Benedetta Carlotti *[a]

In this study, three new push–pull compounds bearing phenothiazine as the electron donor and trithienyltriazine as the electron acceptor connected by triple bond π-bridges and arranged in dipolar (**TRZ1**), quadrupolar (**TRZ2**) and octupolar (**TRZ3**) molecular structures were designed and synthesized. The efficiencies and rates of their excited state deactivation pathways, strongly modulated by the environment, were unveiled through advanced time resolved spectroscopies with nanosecond and femtosecond temporal resolution. Highly efficient fluorescence and intersystem crossing were found to occur in non polar solvents, which justify all the absorbed quanta. Emission measurements in a non polar rigid matrix at low temperature uncovered small singlet-to-triplet energy gaps for these molecules. Indeed, in fairly polar media, an intramolecular charge transfer state quasi-isoenergetic to the triplet excited state was stabilized and populated, resulting in reverse intersystem crossing followed by orange/red delayed fluorescence. Similarly, delayed fluorescence was clearly detected in thin films of **TRZ1–3** at room temperature. Upon increasing the degree of branching among the molecules in this series, the emission color in the solid state was turned from orange to deep red and the amplitude of the delayed component was largely enhanced. The mechanistic reason underlying this behavior could be found in the relatively faster intersystem crossing than prompt fluorescence in the multi-branched compounds. Our results demonstrate the positive role played by the degree of branching in boosting red delayed fluorescence in all-organic materials for applications in third generation organic light emitting diodes.

Received 23rd August 2025,
Accepted 10th November 2025

DOI: 10.1039/d5tc03179f

rsc.li/materials-c

Introduction

Thermally activated delayed fluorescence (TADF) is an intriguing emissive phenomenon exploited in third and fourth generation organic light emitting diodes (OLEDs).[1–6] OLEDs have attracted great interest for display technologies in comparison to traditional liquid crystals for their unique features such as fast response time, thinness, flexibility, transparency, no backlighting, wide viewing angle and low power lighting.[7] Over the past few decades, luminescent materials for OLED devices have undergone development from organic fluorophores (first generation OLEDs based on fluorescence) to organometallic phosphors (second generation OLEDs based on phosphorescence), with internal quantum efficiencies (IQEs) increasing from 25% to 100%. On the other hand, TADF allows to harvest triplet excitons to give delayed fluorescence emission following the reverse intersystem crossing from the triplet to the singlet excited state.[8] TADF-based OLEDs combine the advantage of low cost all-organic fluorescent materials with the high-efficiency of phosphorescent OLEDs.[9] While many examples of blue, green and yellow TADF emitters have been reported in the recent literature, developing effective orange and red TADF fluorophores remains a challenge.[10–18] This is mainly due to the energy gap law: longer emission wavelengths imply a narrower S_1–S_0 energy gap, with the consequent prevalence of nonradiative decay processes. In order to boost the efficiency of red TADF emitters, *ad hoc* molecular design strategies have been developed. Push–pull systems exhibiting strong intramolecular donor (D)–acceptor (A) interactions have been considered to obtain a red-shifted emission and achieve the small singlet-to-triplet energy gap necessary to enable the reverse intersystem crossing process.[19,20] The goal of a significant fluorescence efficiency has been generally pursued by increasing the molecular conjugation of the considered organic molecules.[21,22]

[a] *Department of Chemistry, Biology and Biotechnology and CEMIN, University of Perugia, via Elce di sotto n.8, 06123 Perugia, Italy. E-mail: benedetta.carlotti@unipg.it*
[b] *Department of Chemistry, Indian Institute of Technology, Indore 453552, India. E-mail: rajneeshmisra@iiti.ac.in*
† Equally contributed as first authors.

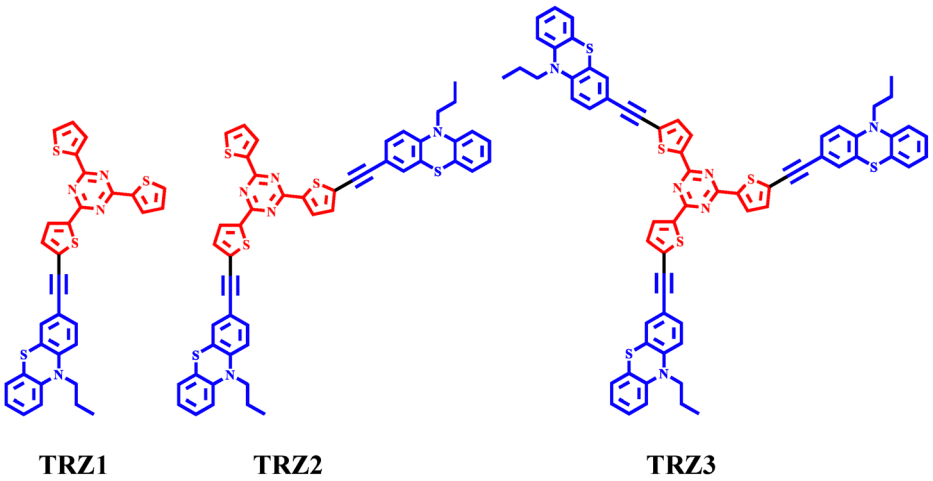

Chart 1 Molecular structures of the investigated compounds.

Our group has recently contributed to the development of new red TADF emitters by synthetizing and characterizing new phenothiazine-naphthalimide derivatives, where the phenothiazine is the electron donor and the naphthalimide the electron acceptor portion.[22,23] In this investigation, we consider a stronger electron acceptor unit, constituted by a triazine derivative. Triazine is indeed a well know structural motif as a remarkable electron acceptor in TADF emitters.[24–30] Previous literature work has described the photophysics of phenothiazine-triphenyltriazine conjugates bearing single bond linkers, highlighting the occurrence of intense yellow TADF.[17,28,29,31–33] In the present work, with the aim being increasing the molecular conjugation to enable efficient orange-red TADF, we synthetized phenothiazine-triazine derivatives bearing triple bonds as π-bridges as well as arranged in dipolar (**TRZ1**), quadrupolar (**TRZ2**) and octupolar (**TRZ3**) structures characterized by different degrees of branching (Chart 1).[34] Moreover, in the molecular structures here considered, the central triphenyltriazine unit was replaced with a trithienyltriazine since that employing thiophenes, instead of phenyls, has been sometimes described in the literature to imply a red shift in the absorption and emission spectra.[35] Here, a comprehensive photophysical study was carried out for the new **TRZ1–3** chromophores, both in solution and in solid state thin films, utilizing state-of-the-art time resolved spectroscopies, such as nanosecond and femtosecond transient absorption and femtosecond broadband fluorescence up conversion. A deep insight was gained into the yields, rates and energetics of the fluorescence and intersystem crossing processes[36,37] of such push–pull compounds, which may inspire future ideas for new optimized red TADF materials for third generation OLEDs based on chemical principles rather than trial-and-error approaches.

Results and discussion

Synthesis and characterization

The synthetic procedure for the **TRZ1–3** derivatives is summarized in Scheme 1 and detailed in the SI. These compounds were synthesized *via* Sonogashira cross-coupling reaction between **Mono-TRZ-Th**, **Di-TRZ-Th**, and **Tri-TRZ-Th** with **PTZ4** in a 1 : 1 mixture of triethylamine and tetrahydrofuran. The reaction was performed at 60 °C in the presence of $Pd(PPh_3)_2Cl_2$ and CuI as catalysts, resulting in **TRZ1–3** in 69%, 57%, and 67% yield, respectively.

All the compounds were purified by column chromatography using hexane:dichloromethane as the eluent and were well-characterized by ^{1}H NMR spectroscopy, ^{13}C NMR spectroscopy, and HRMS techniques (see Fig. S1–S23).

Absorption and emission properties

Fig. 1 shows the absorption and emission spectra of **TRZ1–3** in a non polar solvent, such as cyclohexane. The molecular

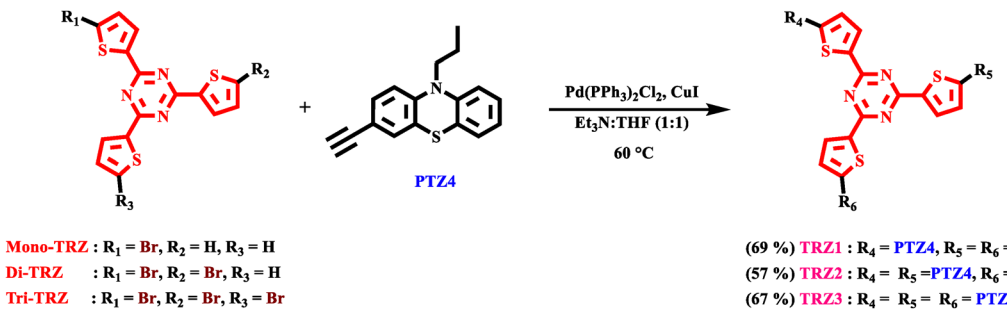

Scheme 1 Synthetic route for triazine-based chromophores **TRZ1–3**.

structure effect on the spectra is small and implies a slight red shift of both the absorption and emission bands upon passing from the mono-branched to the double-branched and tri-branched derivatives. On the other hand, the fluorescence properties (Table 1) were significantly affected by the molecular structure with a fluorescence quantum yield (Φ_F) of 18% for **TRZ1**, 26% for **TRZ2** and 35% for **TRZ3** in cyclohexane. Similarly, the fluorescence lifetime (τ_F) was enhanced on going from **TRZ1** (0.8 ns) to **TRZ2** (1.0 ns) and **TRZ3** (1.2 ns). As a result, the fluorescence rate constant, computed as $k_F = \Phi_F/\tau_F$, was found to be slightly larger in **TRZ3** (2.9×10^8 s^{-1}) relative to **TRZ2** (2.6×10^8 s^{-1}) and **TRZ1** (2.2×10^8 s^{-1}).

The effect of the solvent on the absorption and fluorescence spectra of **TRZ1** is shown in Fig. 1 and detailed in Fig. S26 and S27 for **TRZ2** and **TRZ3**. The absorption spectra undergo a small shift, mainly determined by the solvent polarizability. A very significant red shift is instead observed for the fluorescence spectrum with the solvent dielectric constant.[38,39] The fluorescence spectrum shows an important vibrational structure in the less polar solvents (*n*-hexane and cyclohexane) while becoming a broad structureless band in the relatively more polar toluene, anisole and tetrahydrofuran solvents. This

Table 1 Fluorescence properties of **TRZ1–3** in cyclohexane (upper table) and of **TRZ1** in solvents of different polarities (lower table)

Structure effect in cyclohexane

	Φ_F	τ_F (ns)	k_F (s^{-1})
TRZ1	0.18	0.8	2.2×10^8
TRZ2	0.26	1.0	2.6×10^8
TRZ3	0.35	1.2	2.9×10^8

Solvent effect for **TRZ1**

	ε	Φ_F	τ_F (ns)	k_F (s^{-1})
n-Hexane	1.89	0.13	0.8	1.6×10^8
Cyclohexane	2.02	0.18	0.8	2.2×10^8
Toluene	2.38	0.63	3.3	1.9×10^8
Anisole	4.33	0.23	2.5	9.2×10^7
THF	7.58	0.07	2.0	3.5×10^7
MeCN	36.6	0.001	—	—

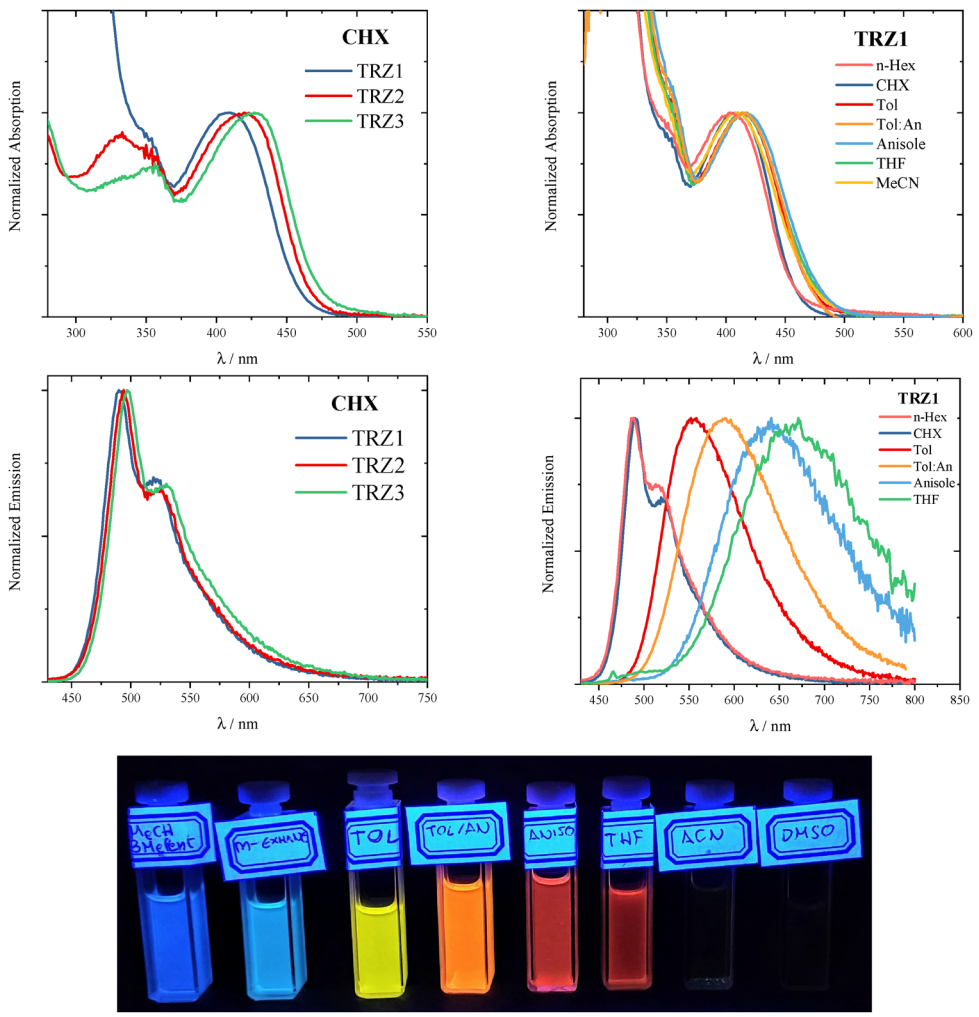

Fig. 1 Normalized Absorption (upper graphs) and Emission (lower graphs) spectra of **TRZ1–3** in cyclohexane (left) and of **TRZ1** in solvents of different polarities (right). To record the emission spectra for each sample, excitation was carried out at the corresponding absorption maximum above 400 nm. Image: Fluorescence of **TRZ1** in different solvents under UV light at 365 nm.

strong positive fluorosolvatochromism implies a significant change in the colour of the emission with the solvent: from the blue fluorescence in *n*-hexane and cyclohexane, to yellow in toluene, orange in a toluene/anisole mixture and red in anisole and tetrahydrofuran (Fig. 1). No significant visible emission was observed in the more polar acetonitrile and dimethylsulfoxide solvents under ultraviolet light. For **TRZ1–3**, the fluorescence spectra recorded in most solvents show of a single emission band (Fig. 1), no significant excitation wavelength effect was observed on the emission spectra (Fig. S29) and the excitation spectra were found to overlap well the relative absorption spectrum (Fig. S25 and S29). The only evidence for a small contribution of a second emitting species (possibly a conformer, as discussed in literature studies about phenothiazine)[29,40] was found while investigating the fluorescence spectra in tetrahydrofuran (Fig. S30). The fluorescence quantum yield was largely affected by the solvent polarity, with similar trends also observed for the fluorescence lifetime and rate constant of **TRZ1–3** (Table 1 and Tables S2–S4). The fluorescence quantum yield was found to increase from 0.13 in *n*-hexane to 0.18 in cyclohexane and 0.63 in toluene for **TRZ1**. Similar fluorescence quantum yields (0.63), lifetimes (3.3 ns) and rate constants (1.9×10^8 s^{-1}) were measured for all the **TRZ1–3** investigated compounds in toluene. This finding suggests that excited state symmetry breaking and localization of the excitation on a single branch of the molecular structure take place for the quadrupolar and octupolar derivatives.[41–43] Upon further increasing the solvent dielectric constant, a significant fluorescence quenching was observed in anisole (Φ_F = 0.23 for **TRZ1**) and tetrahydrofuran (Φ_F = 0.07 for **TRZ1**). This double trend of the fluorescence properties with the solvent dielectric constant indicates the presence of two competitive deactivation pathways to the fluorescence, one operative in non polar media (such as *n*-hexane and cyclohexane) and one operative in polar solvents (anisole and tetrahydrofuran). In particular, in the most polar solvent investigated in detail (tetrahydrofuran) the photoinduced intramolecular charge transfer competitive pathway seems to be more efficient leading to a more effective fluorescence quenching for the octupolar **TRZ3** (Φ_F = 0.02) and for the quadrupolar **TRZ2** (Φ_F = 0.03) than for the dipolar **TRZ1** (Φ_F = 0.07).[44]

Quantum chemical calculations at the DFT level performed on the ground state optimized geometry showed that the $S_0 \rightarrow S_1$ transition is mainly described by the HOMO–LUMO configuration for **TRZ1–3** (Fig. S31 and Tables S5–S8). The electron density of the HOMOs for **TRZ1–3** is displaced over the one/three phenothiazine units and the ethynyl thiophene spacers. As for the LUMOs the electron density is mainly localized on the central thienyl triazine core. The absorption band at longest wavelength are thus characterized by a significant intramolecular charge transfer character. The computationally predicted absorption spectra exhibited a remarkable agreement with the experimental ones (Fig. S32).

The redox potentials of **TRZ1–3** were evaluated by cyclic voltammetry and differential pulse voltammetry (Fig. S33, S34 and Table S9). All the measurements were performed in dry dichloromethane at room temperature using 0.1 M tetrabutylammonium hexafluorophosphate as a supporting electrolyte. The electrochemical behaviour of **TRZ1–3** reveals both oxidation and reduction processes, arising from the incorporation of

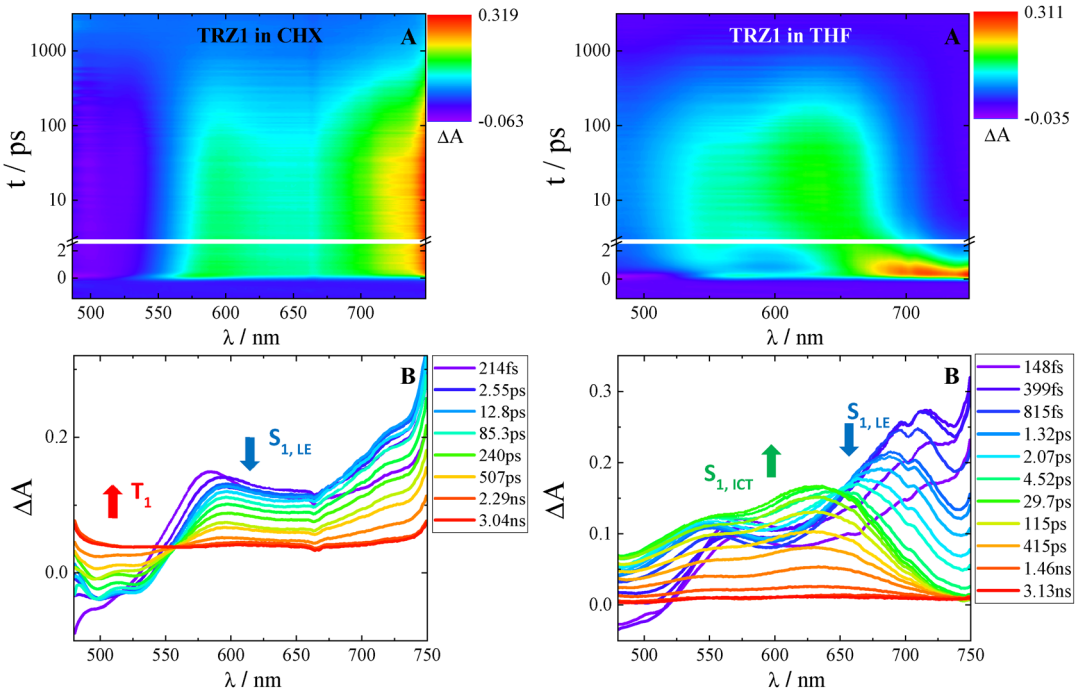

Fig. 2 Femtosecond transient absorption of **TRZ1** in cyclohexane (left) and tetrahydrofuran (right): (A) tridimensional data matrix ΔA as a function of wavelength and time; (B) time resolved absorption spectra at different delays after photoexcitation.

donor and acceptor units within their molecular structures. All the three derivatives exhibit two oxidation waves in the anodic region and two reduction waves in the cathodic region in their cyclic voltammograms. The oxidation waves observed at lower potentials are attributed to the phenothiazine unit,[39] whereas the oxidation wave at higher potentials corresponds to the thiophene spacer.[45] The reduction waves for **TRZ1–3** in the cathodic region are due to the triazine moiety.[46]

Ultrafast spectroscopy

The nature of these non radiative deactivation pathways was unveiled through the investigation of the ultrafast excited state dynamics *via* femtosecond transient absorption and broadband fluorescence up conversion measurements for **TRZ1–3** in selected solvents of different polarities (cyclohexane, toluene and tetrahydrofuran).

The results of the femtosecond transient absorption experiments for **TRZ1** in cyclohexane and tetrahydrofuran are shown in Fig. 2 as representative examples. The transient absorption spectra in cyclohexane at early delays exhibit a broad positive excited state absorption (ESA) band peaked at 575 nm and 710 nm as well as a negative signal due to stimulated emission (SE) peaked around 500 nm. While this transient spectrum decays, a positive broad ESA peaked below 500 nm rises and remains also at long delays after photoexcitation. The fitting of these data revealed the presence of four exponential components (Table 2 and Fig. S35): a first component with a lifetime of 1.6 ps assigned to vibrational cooling (VC), a second component with a lifetime of 240 ps assigned to structural relaxation (SR), a third component with a lifetime of 800 ps in line with the fluorescence decay assigned to the lowest excited singlet state (S_1), a fourth component with an Infinite lifetime as not decaying in the investigated time window of *ca.* 3 ns assigned to the lowest excited triplet state (T_1). Such assignments were confirmed by the fluorescence up conversion experiments (Fig. 3 and Fig. S44–S46 as well as Table 2). In cyclohexane, the time resolved emission spectra highlighted a structured fluorescence centered around 525 nm, formed at early delays after excitation and decaying within the investigated time window of 3 ns. Such emission was assigned to the locally excited singlet state populated upon light absorption ($S_{1,LE}$). The ultrafast experiments in cyclohexane thus undisclosed the occurrence of intersystem crossing for all the **TRZ1–3** compounds, which takes place in 800 ps for **TRZ1**, 1000 ps for **TRZ2** and 1200 ps for **TRZ3** (see Table 2 and Fig. S35–S37).

When **TRZ1** was investigated in the more polar tetrahydrofuran solvent through femtosecond transient absorption (Fig. 2), the initial spectrum characterized by the 550 nm and 710 nm ESA and by the 500 nm SE was found to evolve in time toward another species, not observed in cyclohexane, characterized by an absorption spectrum with broad bands at 530 nm and 630 nm. This transient was then found to decay within the investigated time window. The global fit revealed the presence of five exponential components for **TRZ1** in tetrahydrofuran (Table 2 and Fig. S41): the first two of 0.52 ps and 1.4 ps compatible with solvent relaxation (solv.)[47] and with a spectral shape resembling the $S_{1,LE}$ state, the third component of 300 ps associated to structural relaxation (SR) possibly among different conformers, the forth component of few nanoseconds assigned to an intramolecular charge transfer state ($S_{1,ICT}$) stabilized in this polar solvent, a residual Inf component relative to a still sizable population of the T_1 state. These results were confirmed by the fluorescence up conversion experiments in tetrahydrofuran (Fig. 3 and Fig. S50–S52). The emission spectra temporal dynamics appeared to be completely different from that in the non polar cyclohexane. The spectrum at early delays is a vibrationally structured band at 525 nm, resembling the $S_{1,LE}$ emission. This spectrum then undergoes an important red shift in time. The final emission is constituted by a broad band centered at *ca.* 650 nm and assigned to the $S_{1,ICT}$ in a polar solvent such as tetrahydrofuran.[48] The ultrafast experiments in tetrahydrofuran for **TRZ1**, but also for **TRZ2** and **TRZ3**, unveil the occurrence of intramolecular charge transfer which is, besides intersystem crossing, the other competitive pathway to the fluorescence operative for these molecules in polar solvents. The ultrafast data revealed a $S_{1,ICT}$

Table 2 Lifetimes resulting from the global analysis of the femtosecond transient absorption (TA) and fluorescence up conversion (FUC) data for **TRZ1–3** in cyclohexane (CHX) and tetrahydrofuran (THF)

Solvent	τ / ps						Assignment
	TRZ1		TRZ2		TRZ3		
	TA	FUC	TA	FUC	TA	FUC	
CHX	1.6	4.1	0.95	3.9	0.88	6.2	VC
	240	270	200	290	100	120	SR
	800	800	1000	1000	1200	1200	$S_{1,LE}$
	Inf		Inf		Inf		T_1
THF	0.52	0.51	0.51	0.47	0.71	0.59	Solv.
	1.4	1.5	1.2	1.5	1.4	1.2	Solv./$S_{1,LE}$
	300	180	365	180	265	140	SR
	2000	2000	1400	1400	1400	1400	$S_{1,ICT}$
	Inf		Inf		Inf		T_1

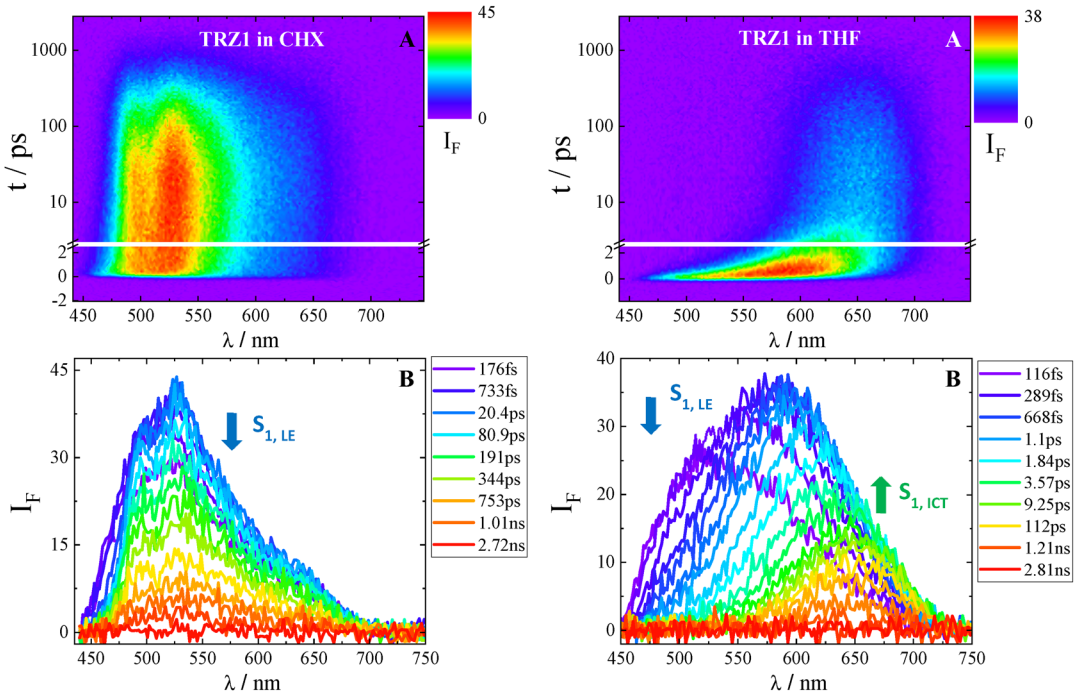

Fig. 3 Femtosecond broadband fluorescence up conversion of **TRZ1** in cyclohexane (left) and tetrahydrofuran (right): (A) tridimensional data matrix fluorescence intensity as a function of wavelength and time; (B) time resolved emission spectra at different delays after photoexcitation.

lifetime of 2.0 ns for **TRZ1** while being 1.4 ns for both **TRZ2** and **TRZ3** in tetrahydrofuran (see Table 2). These findings suggest a faster non radiative deactivation of the ICT excited state to the ground state for the more complex quadrupolar and octupolar structures relative to the dipolar system, in agreement with their smaller fluorescence quantum yields in this solvent.[44]

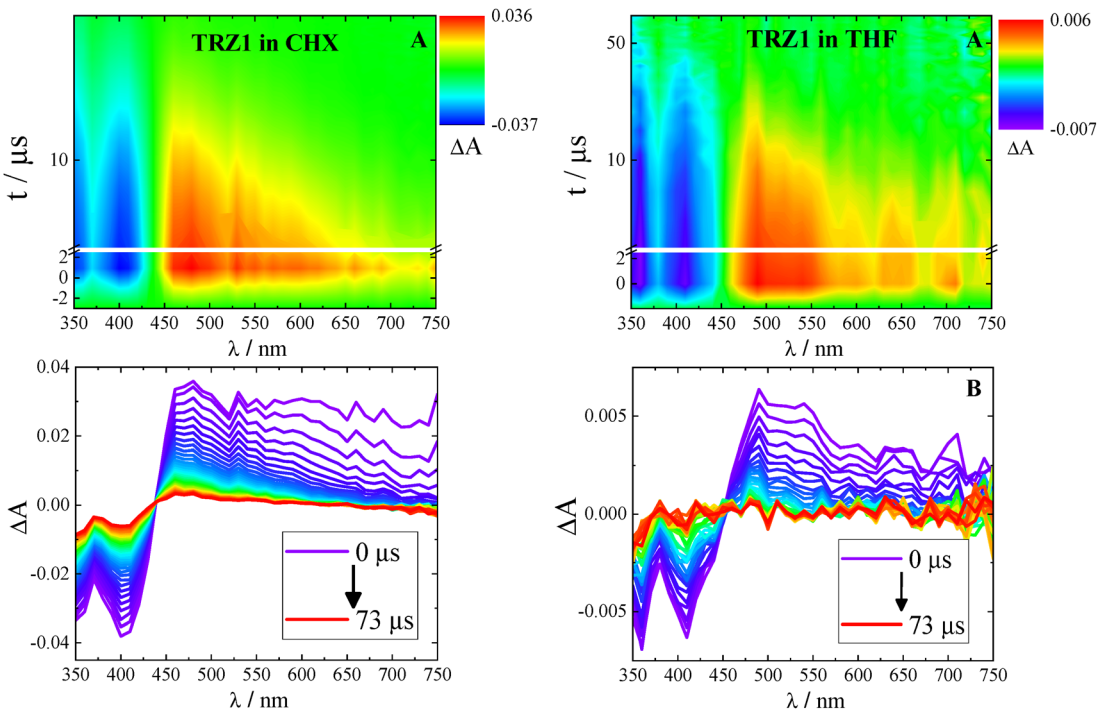

Fig. 4 Nanosecond transient absorption results: (A) tridimensional data matrix Δ*A* as a function of wavelength and time; (B) time resolved absorption spectra at different delays after photoexcitation. Left: **TRZ1** in cyclohexane. Right: **TRZ1** in tetrahydrofuran.

Table 3 Triplet properties of **TRZ1–3** in cyclohexane (upper table); fluorescence and triplet quantum yields for **TRZ1** in solvents of different polarities (lower table)

Structure effect in cyclohexane

Compound	Solvent	$\tau_{T,air}$ (ns)	$\tau_{T,N2}$ (μs)	ε_T (M^{-1} cm^{-1})	Φ_T
TRZ1	CHX	200	25	14 400	0.92
TRZ2		180	42	17 450	0.58
TRZ3		156	40	18 280	0.36

Solvent effect for **TRZ1**

Compound	Solvent	Φ_F	Φ_T
TRZ1	CHX	0.18	0.92
	Tol	0.63	0.22
	THF	0.07	0.05

Triplet properties

The intersystem crossing pathway of triplet formation was investigated in more detail for **TRZ1–3** through nanosecond transient absorption experiments.

The nanosecond transient spectra recorded in cyclohexane (Fig. 4 and Fig. S53) exhibited a region of negative signal due to ground state bleaching (GSB) centered around 400 nm and a broad band of positive ESA peaked at *ca.* 480 nm, with the maximum slightly red shifting upon increasing conjugation in the molecular structure. The ESA peak resulted somehow red shifted (500–520 nm) also when the experiments were carried out in more polar solvents (Fig. S54–S56). The observed transient species was found to decay in hundreds of nanoseconds in air equilibrated and in tens of microseconds in nitrogen purged solution, revealing an exceptional sensitivity to the presence of molecular oxygen (Fig. S57). This transient was found to be successfully sensitized by a high energy triplet donor, such as 2,2′-dithienyl ketone (DTK).[49] These findings proved unambiguously that the detected excited species was the lowest excited triplet state (T_1) of these molecules. Sensitization experiments also allowed to obtain information about the triplet extinction coefficients, found to be 14 400 M^{-1} cm^{-1} for **TRZ1**, 17 450 M^{-1} cm^{-1} for **TRZ2** and 18 280 M^{-1} cm^{-1} for **TRZ3**, slightly enhanced upon increasing molecular conjugation. Relative actinometry measurements allowed to get an accurate evaluation of the triplet quantum yield (Φ_T), which was revealed to be 92% for **TRZ1**, 58% for **TRZ2** and 36% for **TRZ3** in cyclohexane (see Table 3). The triplet yields were observed to significantly decrease upon increasing the solvent dielectric constant (Table S11). While the main decay pathway is the intersystem crossing in cyclohexane (*e.g.* for **TRZ1** Φ_F = 18% and Φ_T = 92%), a relatively more important fluorescence is observed in toluene (*e.g.* for **TRZ1** Φ_F = 63% and Φ_T = 22%). In tetrahydrofuran, both the intersystem crossing and the fluorescence are revealed to be low efficient processes (*e.g.* for **TRZ1** Φ_F = 7% and Φ_T = 5%), pointing to the crucial role played by the intramolecular charge transfer in polar media. Deactivation of the low energetic $S_{1,ICT}$ will likely take place mainly through internal conversion to the ground state for these molecules.

Delayed fluorescence

Information about the singlet and triplet excited state energies was gained through emission measurements at 77 K. Steady and delayed emission spectra were recorded, which should correspond to the fluorescence and phosphorescence spectra under these experimental conditions (Fig. 5 and Fig. S58, S59). Phosphorescence spectra were found to be red shifted relative to the fluorescence and peaked at *ca.* 600 nm for **TRZ1** and *ca.* 650 nm for **TRZ2–3**. The shoulder observed in the delayed spectrum of **TRZ2–3** around 560 nm may be due to some

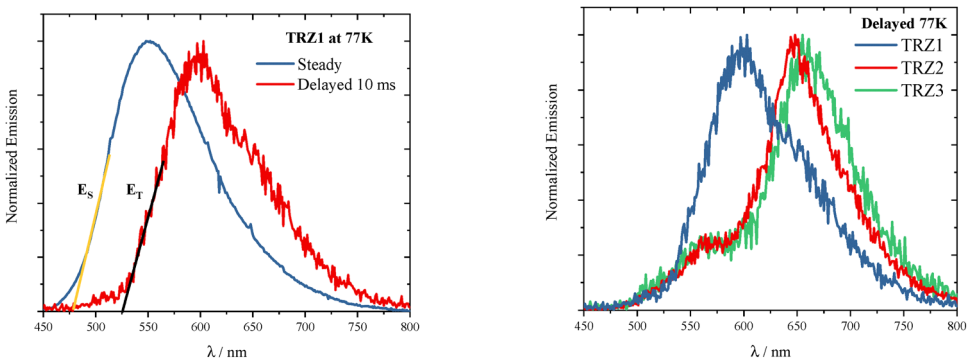

Fig. 5 Emission spectra recorded in MethylCyclohexane/3-MethylPentane mixture at 77 K. Left: Steady and Delayed emission spectra for **TRZ1** and determination of the singlet and triplet excited state energies. Right: Delayed emission spectra for **TRZ1–3**.

Table 4 Singlet (E_S) and triplet (E_T) excited state energies as derived from the steady and delayed emission spectra recorded at 77K (given in nm and in eV) and relative singlet-to-triplet energy gaps (ΔE_{ST} in eV) for **TRZ1–3**

Compound	E_S (nm eV^{-1})	E_T (nm eV^{-1})	ΔE_{ST} (eV)
TRZ1	479/2.59	525/2.36	0.23
TRZ2	489/2.54	575/2.16	0.38
TRZ3	504/2.46	591/2.10	0.36

delayed fluorescence following triplet–triplet annihilation, as also reported in literature studies.[8] From the onset of the fluorescence and phosphorescence spectra, the singlet and triplet excited state energies were evaluated, respectively (see Fig. 5 left). Both the singlet and triplet excited state energies were found to decrease upon increasing the molecular branching on going from **TRZ1** to **TRZ2** to **TRZ3** (Table 4). The singlet-to-triplet energy gaps (ΔE_{ST}) were found to be in the range 0.23–0.38 eV, compatible with the occurrence of thermally activated delayed fluorescence.[50]

The significant intersystem crossing observed for these all-organic compounds and the rather small ΔE_{ST} pushed us to investigate further their delayed fluorescence ability. Therefore, fluorescence decay kinetics were recorded on long time scales of 1–2 μs through the Time correlated single photon counting (TC-SPC) technique. In rather polar solvents, such as tetrahydrofuran, a clear biexponential decay was observed (Fig. 6 left and Fig. S61), with a lifetime of few nanoseconds assigned to the prompt fluorescence also detected in a shorter time window (see Fig. S28) as well as a lifetime of 350–370 ns (Table S13). This longer lifetime was found to be consistent with the triplet lifetime measured *via* nanosecond laser flash photolysis in air equilibrated solutions (Table S11). The amplitude of this long lived component in describing the fluorescence decay was found to increase on going from **TRZ1** (0.01%) and **TRZ2** (2%) to **TRZ3** (26%, see Table S13). Interestingly, in the case of **TRZ1**, for which a relatively smaller energy gap and a blue shifted phosphorescence was found, such long lived emission was observed also in solvents of lower polarity, such as toluene and anisole (Fig. S61). The long lived emission detected for **TRZ1–3** at room temperature through these experiments was assigned to delayed fluorescence occurring from the singlet excited state following reverse intersystem crossing from T_1. Given the small but still sizable ΔE_{ST} measured in the low polar methylcyclohexane/3-methylpentane mixture between the $S_{1,LE}$ and T_1 for these compounds, it is likely that the zero gap condition favouring reverse intersystem crossing and delayed fluorescence is achieved at room temperature between the $S_{1,ICT}$ stabilized in more polar solvents (such as anisole and tetrahydrofuran) and the T_1,[51] as sketched in Fig. 7. Indeed, in literature studies, it has been found that polar solvents tend to stabilize S_1 states, while the receiver triplet is much less sensitive to solvent effects.[23,52–54] By comparing the highly solvatochromic fluorescence and the phosphorescence spectra recorded for **TRZ2–3**, it can be inferred that this energy match is achieved in tetrahydrofuran (Fig. S60). Given the blue shifted phosphorescence measured for **TRZ1**, it is feasible that the reverse intersystem crossing becomes energetically possible even in solvents of lower polarity (*e.g.* toluene or toluene/anisole) in this case (Fig. S60). In Fig. 7, histograms giving the detailed rate constant values of prompt fluorescence ($k_{PF} = \phi_F/\tau_{S_1}$) and intersystem crossing ($k_{ISC} = \phi_T/\tau_{S_1}$) for **TRZ1–3** in tetrahydrofuran, where an apparent delayed fluorescence is observed, are also reported. It is noteworthy that the computed k_{PF} and k_{ISC} are of the same order of magnitude for all the three compounds. Interestingly, k_{PF} is larger than k_{ISC} for **TRZ1** ($k_{PF} = 3.5 \times 10^7$ s^{-1} and $k_{ISC} = 2.5 \times 10^7$ s^{-1}), k_{PF} is equal to k_{ISC} for **TRZ2** ($k_{PF} = 2.1 \times 10^7$ s^{-1} and $k_{ISC} = 2.1 \times 10^7$ s^{-1}) and k_{PF} is lower than k_{ISC} for **TRZ3** ($k_{PF} = 1.4 \times 10^7$ s^{-1} and $k_{ISC} = 3.6 \times 10^7$ s^{-1}). The larger k_{PF} for **TRZ1** compared to **TRZ2** and **TRZ3** in tetrahydrofuran may be due to its relatively lower excited state intramolecular charge transfer degree. These data give a justification to why, under these experimental conditions of roughly zero ΔE_{ST} in tetrahydrofuran, a more important delayed fluorescence is observed for **TRZ3** than for **TRZ2** than for **TRZ1**.[55,56] A method described in the literature by Monkman *et al.*[8] was employed to obtain an estimate of the reverse intersystem crossing rate constant (k_{rISC}) for the investigated compounds. The employed method and the obtained results are reported in detail in Table S14. The obtained k_{rISC} values are

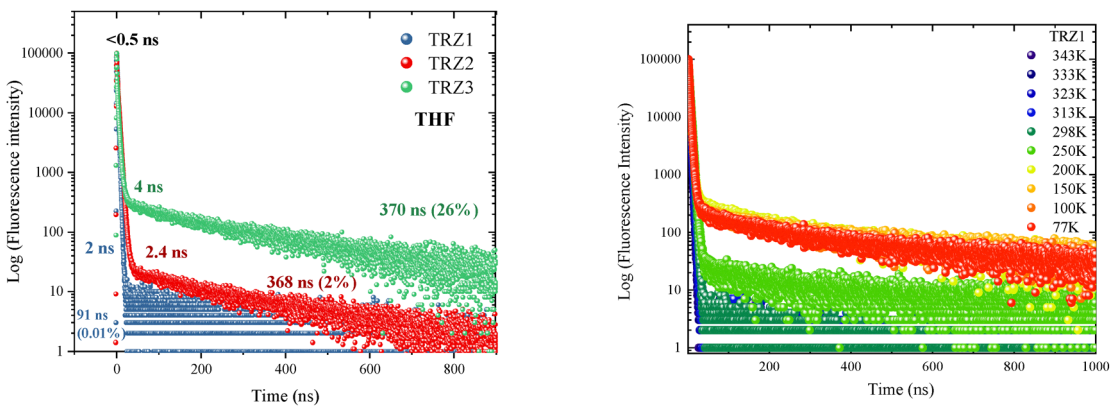

Fig. 6 Fluorescence decay kinetics recorded on a long time window (1–2 μs) through the time correlated single photon counting technique for **TRZ1–3** in tetrahydrofuran (THF) at room temperature (left) and for **TRZ1** in toluene at different temperatures in the 77–343 K range (right).

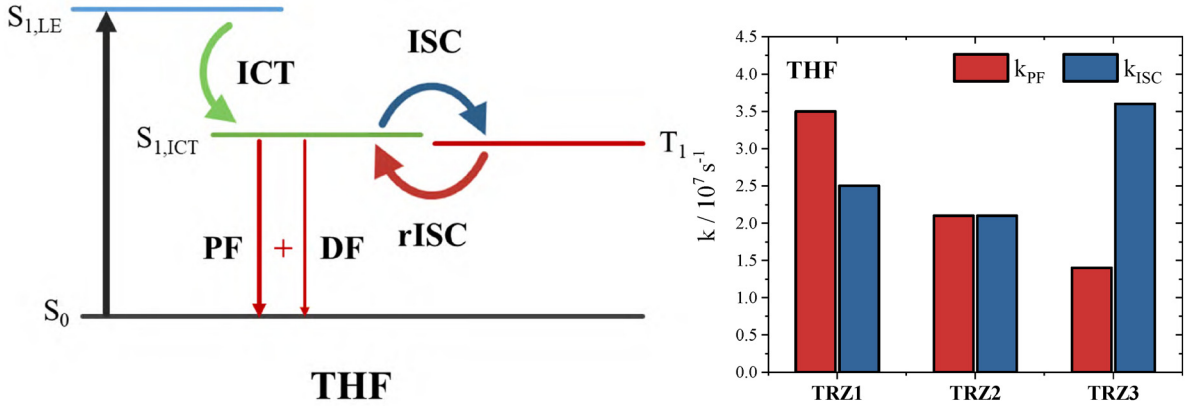

Fig. 7 Left: Sketch of the excited state deactivation for the investigated compounds in tetrahydrofuran (THF). Right: Histogram detailing the prompt fluorescence (k_{PF}) and intersystem crossing (k_{ISC}) rate constants for **TRZ1–3** in tetrahydrofuran.

quite low but show a trend of increasing upon increasing the degree of branching and suggest that **TRZ2** and **TRZ3** may be considered TADF materials (k_{rISC} = 1.1 × 10^5 and 5.9 × 10^5 s^{-1}, respectively).

The effect of temperature on the fluorescence decay kinetics in toluene was investigated to gain information about the thermally activated delayed fluorescence behaviour of these molecules.[57] At 77 K, in a rigid frozen toluene matrix, the fluorescence kinetics shows a clear biexponential decay for all the **TRZ1–3** with the prompt fluorescence exhibiting lifetimes of few nanoseconds and a delayed fluorescence component in the hundreds of nanoseconds timescale (Fig. S62 and Table S15). For **TRZ1** (Fig. 6), the importance of such long lived component was found to be large and slightly enhanced upon raising the temperature up until 200 K, pointing to the thermal activation of the delayed fluorescence behaviour. At higher temperatures, when the toluene matrix begins to melt becoming a liquid environment, the delayed fluorescence was found to be less important (250 K) and then disappear (above room temperature), being possibly turned off by the competition of non radiative decay pathways in this case. When the other chromophores are considered (Fig. S62 and Table S15), the activation of the delayed fluorescence is apparent only between 77 K and 150 K (for **TRZ2**) and only between 77 K and 100 K (for **TRZ3**). This suggests that the competition of non radiative decay pathways in liquid solution may play a more crucial role in such more complex and flexible quadrupolar and octupolar structures compared to **TRZ1**.

Long lived emission in thin film

The three investigated molecules were also characterized for their absorption and emission properties in the solid state, in neat thin films prepared by spin coating. The absorption spectra of the films were found to be red shifted with respect

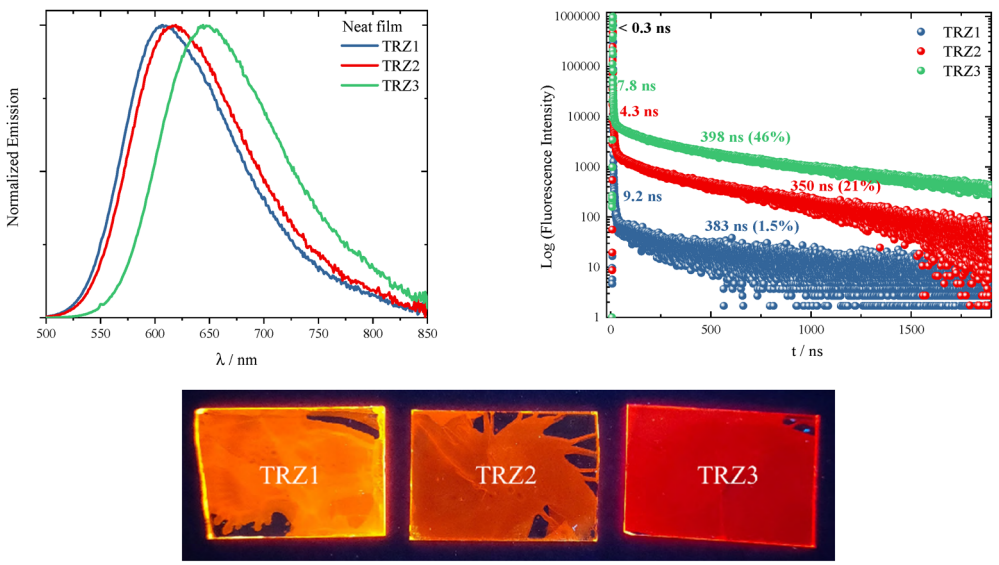

Fig. 8 Normalized fluorescence spectra (upper left graph) and fluorescence decay kinetics on a long time window (upper right graph) for **TRZ1–3** in thin film. Lower image: Fluorescence of **TRZ1–3** films under UV light.

to the solution spectra (Fig. S64). Moreover, both the absorption and the emission bands were found to be red shifted when passing from **TRZ1** to **TRZ2** to **TRZ3**, in line with the increase of branching in this series of molecules (Fig. 7 and Fig. S63). Emission in the neat films was found to be quite intense (quantum yields in Table S16) and centered at 605 nm for **TRZ1**, 620 nm for **TRZ2** and 650 nm for **TRZ3** (Fig. 8). This results in a bright orange to red emission for the thin films observed under ultraviolet light (Fig. 8). Interestingly, nanosecond transient absorption revealed a significant signal decaying with a lifetime of *ca.* 260 ns and characterized by a spectrum showing ground state bleaching around 430 nm and excited state absorption around 540 nm, both slightly red shifted relative to the solution spectrum (Fig. S67). Such kinetic and spectral features suggest that a significant triplet production occurs also in the solid state for **TRZ1**. The remarkable matching between the spectral position of the steady-state fluorescence of the films of **TRZ1–3** and their phosphorescence at low temperature (Fig. S68) pushed us to go deeper into their possible delayed fluorescence capability. Indeed, the fluorescence kinetics of the films were found to show a biexponential decay, with the long component showing a lifetime of 350–400 ns slightly dependent on the molecular structure (Table S17). It is noteworthy that the weight of the delayed fluorescence was found to increase upon passing from **TRZ1** (1.5%) to **TRZ2** (21%) to **TRZ3** (46%) and thus upon increasing the number of branches in the molecular structure of these triazine-phenothiazine fluorophores. The observation of a bright orange-red delayed fluorescence in such novel organic materials in the solid state is highly promising for their possible application in third generation OLED devices.

Further investigation of these films by using a micropulsed lamp and detecting their time resolved emission spectra (TRES) in the microsecond time scale allowed to observe, for the case of **TRZ1**, a long lasting emission characterized by lifetimes of *ca.* 50 μs (see Fig. S70), while the kinetics recorded for the **TRZ2** and **TRZ3** films roughly overlap the instrumental response function. For **TRZ1**, for which a less efficient delayed fluorescence relative to the other investigated fluorophores takes place according to the single photon counting kinetics, the long lived emission observed in film with the TRES analysis matches the phosphorescence centered around 600 nm detected at low temperature (Fig. S69). These findings point to the contribution of room temperature phosphorescence (RTP) in this solid state material on long time windows,[33,38,58,59] which makes its potential for optoelectronic applications high.

Conclusions

In this study, three new push–pull compounds were designed and synthetized bearing trithienyltriazine as the electron acceptor and phenothiazine as the electron donor units, connected by triple bond π-bridges and arranged in dipolar (**TRZ1**), quadrupolar (**TRZ2**) and octupolar (**TRZ3**) structures. The goal of the synthetic effort has been to achieve strong donor–acceptor interactions and large conjugation in these molecules (through the π-linkers and upon increasing the degree of branching) to enable efficient long wavelength delayed fluorescence in these all-organic materials.

The dynamics of fluorescence and intersystem crossing were unveiled for these fluorophores to be strongly modulated by the environment through femtosecond and nanosecond transient absorption as well as femtosecond fluorescence up conversion experiments. Highly efficient fluorescence and intersystem crossing were revealed to be operative in non polar solvents. Fairly small singlet-to-triplet energy gaps (0.23–0.38 eV) were found through emission measurements in rigid matrix at low temperature. In fairly polar solvents, such as anisole or tetrahydrofuran, a stabilized intramolecular charge transfer state is populated, which becomes isoenergetic to the triplet excited state. Consequently, orange/red delayed fluorescence was clearly observed for **TRZ1–3** at room temperature in such media. The relative rates of prompt fluorescence and intersystem crossing for the three molecules point to a relatively faster intersystem crossing than prompt fluorescence for the octupolar compound compared to the quadrupolar and dipolar molecules, justifying the larger amplitude of the delayed fluorescence observed for the three-branched molecule. Interestingly, orange emission was also detected for **TRZ1** thin films. A more important and red delayed fluorescence was revealed for the two branched (**TRZ2**) and three branched (**TRZ3**) derivatives in the solid state, demonstrating the positive impact of increasing the degree of branching on boosting the red delayed fluorescence of these new organic materials. On the other hand, a long lived emission, which could be ascribed to room temperature phosphorescence, was detected for the dipolar **TRZ1** molecule in the solid state. Our results suggest that these new all-organic materials are highly promising for harvesting triplet excitons in optoelectronic light emitting devices to give either bright orange room temperature phosphorescence or red thermally activated delayed fluorescence, depending on the degree of branching of their molecular structure.

Author contributions

P. M., C. M. and K. Y.: data curation, investigation, methodology, writing – original draft, writing – review & editing; E. L.: data curation, investigation, writing – review & editing; R. M.: conceptualization, supervision, writing – review & editing; B. C.: conceptualization, investigation, supervision, writing – original draft, writing – review & editing.

Conflicts of interest

There are no conflicts to declare.

Data availability

The data supporting this article have been included as part of the supplementary information (SI). Supplementary information: Details about the synthesis and characterization (NMR and

HRMS) of the compounds; the absorption and emission properties; the quantum chemical calculations; the electrochemical properties; the ultrafast spectroscopy and laser flash photolysis results; the temperature effect study; the thin film characterization. See DOI: https://doi.org/10.1039/d5tc03179f.

Acknowledgements

This work was financially supported by the European Union - NextGenerationEU under the Italian Ministry of University and Research (MUR) National Innovation Ecosystem grant ECS00000041 – VITALITY and by the MUR under the PRIN 2022 program (grant no. 2022RRFJC4). R. M. acknowledges the Science and Engineering Research Board (SERB) Project No. CRG/2022/000023 and STR/2022/000001, the Council of Scientific and Industrial Research (Project No. 01/3112/23/EMR-II) and STR/2022/000001, New Delhi and the Department of Science and Technology DST-EMR Project No. DST-EMR: EMR/2017/001637.We are grateful to the DST-FIST grant for the 500 MHz NMR facility and the Sophisticated Instrumentation Centre (SIC), Indian Institute of Technology (IIT) Indore. K. Y. thanks the University Grant Commission (UGC)-New Delhi for the fellowship.

Notes and references

1 Y. Liu, C. Li, Z. Ren, S. Yan and M. R. Bryce, *Nat. Rev. Mater.*, 2018, **3**, 1–20.
2 H. Uoyama, K. Goushi, K. Shizu, H. Nomura and C. Adachi, *Nature*, 2012, **492**, 234–238.
3 Y. Im, M. Kim, Y. J. Cho, J.-A. Seo, K. S. Yook and J. Y. Lee, *Chem. Mater.*, 2017, **29**, 1946–1963.
4 M. Y. Wong and E. Zysman-Colman, *Adv. Mater.*, 2017, **29**, 1605444.
5 Z. Yang, Z. Mao, Z. Xie, Y. Zhang, S. Liu, J. Zhao, J. Xu, Z. Chi and M. P. Aldred, *Chem. Soc. Rev.*, 2017, **46**, 915–1016.
6 X.-K. Chen, D. Kim and J.-L. Brédas, *Acc. Chem. Res.*, 2018, **51**, 2215–2224.
7 G. Hong, X. Gan, C. Leonhardt, Z. Zhang, J. Seibert, J. M. Busch and S. Bräse, *Adv. Mater.*, 2021, **33**, 2005630.
8 F. B. Dias, T. J. Penfold and A. P. Monkman, *Methods Appl. Fluoresc.*, 2017, **5**, 012001.
9 F. B. Dias, K. N. Bourdakos, V. Jankus, K. C. Moss, K. T. Kamtekar, V. Bhalla, J. Santos, M. R. Bryce and A. P. Monkman, *Adv. Mater.*, 2013, **25**, 3707–3714.
10 L. Ge, W. Zhang, Y.-H. Hao, M. Li, Y. Liu, M. Zhou and L.-S. Cui, *J. Am. Chem. Soc.*, 2024, **146**, 32826–32836.
11 S. Kothavale, W. J. Chung and J. Y. Lee, *J. Mater. Chem. C*, 2021, **9**, 528–536.
12 Y. Xiao, H. Wang, Z. Xie, M. Shen, R. Huang, Y. Miao, G. Liu, T. Yu and W. Huang, *Chem. Sci.*, 2022, **13**, 8906–8923.
13 Z. Cai, X. Wu, H. Liu, J. Guo, D. Yang, D. Ma, Z. Zhao and B. Z. Tang, *Angew. Chem., Int. Ed.*, 2021, **60**, 23635–23640.
14 J. H. Kim, J. H. Yun and J. Y. Lee, *Adv. Opt. Mater.*, 2018, **6**, 1800255.
15 X. Zhang, X. Liu, M. Taddei, L. Bussotti, I. Kurganskii, M. Li, X. Jiang, L. Xing, S. Ji, Y. Huo, J. Zhao, M. Di Donato, Y. Wan, Z. Zhao and M. V. Fedin, *Chem. – Eur. J.*, 2022, **28**, e202200510.
16 G. Tang, A. A. Sukhanov, J. Zhao, W. Yang, Z. Wang, Q. Liu, V. K. Voronkova, M. Di Donato, D. Escudero and D. Jacquemin, *J. Phys. Chem. C*, 2019, **123**, 30171–30186.
17 L. An, R. Su, Y. Sun, C. Song and Q. Wang, *Comput. Theor. Chem.*, 2023, **1228**, 114277.
18 C. Montanari, M. Sheokand, A. Cesaretti, E. Calzoni, R. Misra and B. Carlotti, *J. Phys. Chem. C*, 2024, **128**, 19688–19700.
19 H. Tanaka, K. Shizu, H. Nakanotani and C. Adachi, *Chem. Mater.*, 2013, **25**, 3766–3771.
20 E. Duda, D. Hall, S. Bagnich, C. L. Carpenter-Warren, R. Saxena, M. Y. Wong, D. B. Cordes, A. M. Z. Slawin, D. Beljonne, Y. Olivier, E. Zysman-Colman and A. Köhler, *J. Phys. Chem. B*, 2022, **126**, 552–562.
21 X.-Y. Zeng, Y.-Q. Tang, J.-X. Zhou, K. Zhang, H.-Y. Wang, Y.-Y. Zhu, Y.-Q. Li and J.-X. Tang, *ACS Appl. Mater. Interfaces*, 2024, **16**, 16563–16572.
22 C. Montanari, N. Ji Tiwari, R. Misra and B. Carlotti, *Chem. – Eur. J.*, 2024, **30**, e202402294.
23 C. Montanari, T. Bianconi, M. Sheokand, T. Teunens, G. Cavalletti, J. Cornil, R. Misra and B. Carlotti, *J. Mater. Chem. C*, 2023, **11**, 10893–10904.
24 H.-Y. Chih, Y.-W. Chen, Y.-C. Hsieh, W.-C. Li, C.-W. Liao, C.-H. Lin, T.-Y. Chiu, W.-W. Tsai, C.-W. Lu and C.-H. Chang, *Chem. – Eur. J.*, 2019, **25**, 16699–16711.
25 S. Kumar, P. Rajamalli, D. B. Cordes, A. M. Z. Slawin and E. Zysman-Colman, *Asian J. Org. Chem.*, 2020, **9**, 1277–1285.
26 T. Serevičius, T. Nakagawa, M.-C. Kuo, S.-H. Cheng, K.-T. Wong, C.-H. Chang, R. C. Kwong, S. Xia and C. Adachi, *Phys. Chem. Chem. Phys.*, 2013, **15**, 15850.
27 D. Sun, C. Si, T. Wang and E. Zysman-Colman, *Adv. Photonics Res.*, 2022, **3**, 2200203.
28 X.-F. Tan, P.-P. Wang, L. Lu, O. Bezvikonnyi, D. Volyniuk, J. V. Grazulevicius and Q.-H. Zhao, *Dyes Pigm.*, 2020, **173**, 107793.
29 H. Tanaka, K. Shizu, H. Nakanotani and C. Adachi, *J. Phys. Chem. C*, 2014, **118**, 15985–15994.
30 D. Sun, E. Duda, X. Fan, R. Saxena, M. Zhang, S. Bagnich, X. Zhang, A. Köhler and E. Zysman-Colman, *Adv. Mater.*, 2022, **34**, 2110344.
31 I. Marghad, F. Bencheikh, C. Wang, S. Manolikakes, A. Rérat, C. Gosmini, D. Hyeon Kim, J.-C. Ribierre and C. Adachi, *RSC Adv.*, 2019, **9**, 4336–4343.
32 I. Marghad, D. H. Kim, X. Tian, F. Mathevet, C. Gosmini, J.-C. Ribierre and C. Adachi, *ACS Omega*, 2018, **3**, 2254–2260.
33 S. A. Elgadi, D. M. Mayder, R. Hojo and Z. M. Hudson, *Adv. Opt. Mater.*, 2023, **11**, 2202754.
34 D. Sun, R. Saxena, X. Fan, S. Athanasopoulos, E. Duda, M. Zhang, S. Bagnich, X. Zhang, E. Zysman-Colman and A. Köhler, *Adv. Sci.*, 2022, **9**, 2201470.
35 L. Fisher Jr, R. J. Vázquez, M. Howell, A. K. Muthike, M. E. Orr, H. Jiang, B. Dodgen, D. R. Lee, J. Y. Lee,

P. Zimmerman and T. I. Goodson, *Chem. Mater.*, 2022, **34**, 2161–2175.
36 R. J. Vázquez, H. Kim, P. M. Zimmerman and T. Goodson, *J. Mater. Chem. C*, 2019, **7**, 4210–4221.
37 R. J. Vázquez, J. H. Yun, A. K. Muthike, M. Howell, H. Kim, I. K. Madu, T. Kim, P. Zimmerman, J. Y. Lee and T. G. Iii, *J. Am. Chem. Soc.*, 2020, **142**, 8074–8079.
38 T. Bianconi, A. Cesaretti, P. Mancini, N. Montegiove, E. Calzoni, A. Ekbote, R. Misra and B. Carlotti, *J. Phys. Chem. B*, 2023, **127**, 1385–1398.
39 Y. Rout, C. Montanari, E. Pasciucco, R. Misra and B. Carlotti, *J. Am. Chem. Soc.*, 2021, **143**, 9933–9943.
40 D.-G. Chen, T.-C. Lin, Y.-A. Chen, Y.-H. Chen, T.-C. Lin, Y.-T. Chen and P.-T. Chou, *J. Phys. Chem. C*, 2018, **122**, 12215–12221.
41 E. Balanikas, T. Bianconi, P. Mancini, N. Ji Tiwari, M. Sheokand, R. Misra, B. Carlotti and E. Vauthey, *Chem. Sci.*, 2025, **16**, 8443–8453.
42 M. Söderberg, B. Dereka, A. Marrocchi, B. Carlotti and E. Vauthey, *J. Phys. Chem. Lett.*, 2019, **10**, 2944–2948.
43 F. Terenziani, A. Painelli, C. Katan, M. Charlot and M. Blanchard-Desce, *J. Am. Chem. Soc.*, 2006, **128**, 15742–15755.
44 F. Ricci, B. Carlotti, B. Keller, C. Bonaccorso, C. G. Fortuna, T. Goodson, F. Elisei and A. Spalletti, *J. Phys. Chem. C*, 2017, **121**, 3987–4001.
45 P. K. Gupta, F. Khan and R. Misra, *J. Org. Chem.*, 2023, **88**, 14308–14322.
46 J. Wang, G. Ouyang, Y. Wang, X. Qiao, W.-S. Li and H. Li, *Chem. Commun.*, 2020, **56**, 1601–1604.
47 M. L. Horng, J. A. Gardecki, A. Papazyan and M. Maroncelli, *J. Phys. Chem.*, 1995, **99**, 17311–17337.
48 Y. Wang, G. S. He, P. N. Prasad and T. Goodson, *J. Am. Chem. Soc.*, 2005, **127**, 10128–10129.
49 F. Ortica, A. Romani and G. Favaro, *J. Phys. Chem. A*, 1999, **103**, 1335–1341.
50 X. Yin, Y. He, X. Wang, Z. Wu, E. Pang, J. Xu and J. Wang, *Front. Chem.*, 2020, **8**(725), 1–23.
51 R. Dhali, D. K. A. Phan Huu, F. Terenziani, C. Sissa and A. Painelli, *J. Chem. Phys.*, 2021, **154**, 134112.
52 Ó. Guzmán-Méndez, M. M. Reza, B. Meza, J. Jara-Cortés and J. Peón, *J. Phys. Chem. B*, 2023, **127**, 5655–5667.
53 E. F. Plaza-Medina, W. Rodríguez-Córdoba and J. Peon, *J. Phys. Chem. A*, 2011, **115**, 9782–9789.
54 W. Rodríguez-Córdoba, L. Gutiérrez-Arzaluz, F. Cortés-Guzmán and J. Peon, *Chem. Commun.*, 2021, **57**, 12218–12235.
55 J. Yang, M. Fang and Z. Li, *Aggregate*, 2020, **1**, 6–18.
56 J. Guo, J. Fan, L. Lin, J. Zeng, H. Liu, C.-K. Wang, Z. Zhao and B. Z. Tang, *Adv. Sci.*, 2019, **6**, 1801629.
57 X. Chen, S. Bagnich, R. Pollice, B. Li, Y. Zhu, R. Saxena, Y. Yin, W. Zhu, A. Aspuru-Guzik, E. Zysman-Colman, A. Köhler and Y. Wang, *Adv. Opt. Mater.*, 2024, **12**, 2301784.
58 C. Chen, R. Huang, A. S. Batsanov, P. Pander, Y.-T. Hsu, Z. Chi, F. B. Dias and M. R. Bryce, *Angew. Chem.*, 2018, **130**, 16645–16649.
59 W. Dai, T. Bianconi, E. Ferraguzzi, X. Wu, Y. Lei, J. Shi, B. Tong, B. Carlotti, Z. Cai and Y. Dong, *ACS Mater. Lett.*, 2021, 1767–1777.

